Nonlinear Landau-Zener-Stückelberg-Majorana interferometry

Sheng-Chang Li,[1,*] Li-Bin Fu,[2,4] and Jie Liu[3,4]

[1]*School of Science, Xi'an Jiaotong University, Xi'an 710049, China and Shaanxi Province Key Laboratory of Quantum Information and Quantum Optoelectronic Devices, Xi'an Jiaotong University, Xi'an 710049, China*

[2]*Graduate School, China Academy of Engineering Physics, Beijing 100193, China*

[3]*Laboratory of Computational Physics, Institute of Applied Physics and Computational Mathematics, Beijing 100088, China*

[4]*HEDPS, CAPT, and CICIFSA MoE, Peking University, Beijing 100871, China*

(Received 21 May 2018; published 2 July 2018)

We investigate Landau-Zener-Stückelberg-Majorana (LZSM) interferometry in a nonlinear two-level system subjected to a sinusoidal driving field. A comprehensive analysis for the interference patterns is shown from which we can analytically obtain the condition of constructive and destructive interferences in some cases. In the presence of nonlinear interaction, the level structure is changed, which can lead to an asymmetric deformation of the interference patterns and a significant position shift of the interference fringes. Our findings suggest an application of the nonlinear LZSM interferometry in accurately calibrating the parameters characterizing a nonlinear two-level system, as well as its coupling with the driven fields.

DOI: 10.1103/PhysRevA.98.013601

I. INTRODUCTION

The quantum two-level (TL) model plays an important role in describing various physical systems. The famous Landau-Zener (LZ) transition is often known as the transition between two levels at an avoided crossing [1,2]. When one imposes strongly periodic driving on a TL system, a sequence of LZ transitions occurs and the physical observables exhibit periodic dependence on the phase (known as the Stückelberg phase) accumulated between the transitions [3,4]. This periodicity (illustrated by interference fringes) is called Stückelberg oscillations, which provide the basis of Landau-Zener-Stückelberg-Majorana (LZSM) interferometry [5–7]. The increasing attention is focused on LZSM interferometry because it can be used to characterize qubit dephasing [8], probe the coherent coupling of two dopants in a silicon nanowire [9], realize ultrafast quantum control of a qubit [10], and so on. In the last few decades, LZSM interference has been studied in a number of physical systems and served as a textbook model for quantum phenomena [5], such as the studies on related LZSM interference or Stückelberg oscillations in semiconductor superlattices [11,12], superconducting quantum point contacts [13], superconducting qubits [14], magnetic molecules [15,16], molecular nanomagnets [17–19], nitrogen vacancy centers in diamond [20,21], quasi-one-dimensional layered materials [22,23], ultracold molecules [24,25], Rydberg atoms [26], Bose-Einstein condensates (BEC) [27,28], etc. Recently, the effects of quantum noise on LZSM interferometry [29], the spatial LZSM interference [30], the pseudo-Hermitian LZSM model [31], and the exactly solvable model for LZSM interferometry [32] have been investigated.

Most of works on LZSM interferometry were addressed with LZ theory considering either no particle-particle interaction or weak interaction. However, when we discuss LZSM, for example, in atomic BEC systems, the many-body effect of atom-atom interaction should be taken into account, and this interaction in some cases is very strong. A variety of nonlinear interactions between particles may produce unexpected quantum tunneling [33–35] and interference [36–38] features. For instance, it was shown that the frequency shift of the interference fringes strongly depends on the type and strength of the particle interaction [38]. In this paper, we study the influence of the nonlinear interaction on LZSM interferometry by employing a nonlinear periodic driven two-level model which can be used to describe a two-mode (or double-well) atomic BEC system at a mean-field level [39,40]. It is found that the symmetry, the position, the width, and the intensity of the interference fringes are sensitive to the nonlinear interaction and can be strongly modified by the nonlinear interaction. These effects provide good opportunity to precisely measure the interaction between particles in many-body systems and the coupling between such systems and external control fields.

The paper is organized as follows. In Sec. II we describe the model that we adopt, namely, the periodically driven nonlinear two-level model. In Sec. III we present the main results of this paper. The nonlinear LZSM interferometry is categorized into four cases, namely, weak-coupling, strong-coupling, weak-driving, and strong-driving limits. Finally, we briefly discuss the experimental possibility of our theoretical findings and summarize the results in Sec. IV.

II. NONLINEAR TWO-LEVEL MODEL

The model Hamiltonian of a nonlinear two-level system under temporally periodic driving reads ($\hbar = 1$) [33,34]

$$H(t) = \frac{\Delta}{2}\hat{\sigma}_x + \frac{\gamma(t) + c(|b|^2 - |a|^2)}{2}\hat{\sigma}_z, \tag{1}$$

*scli@mail.xjtu.edu.cn

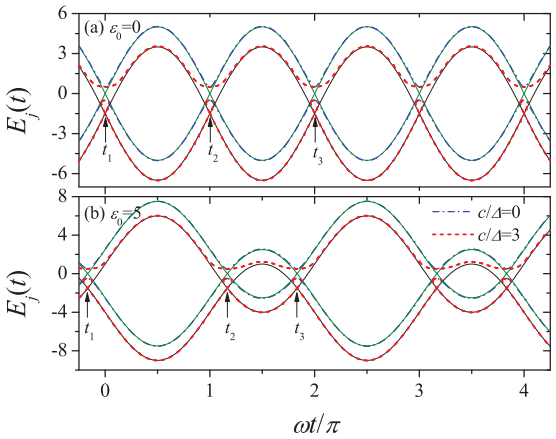

FIG. 1. Time evolution of the energy levels for different offsets: (a) $\epsilon_0 = 0$ and (b) $\epsilon_0 = 5$. The time-dependent adiabatic energy levels (i.e., $\Delta = 1$) are plotted by the thick dashed-dotted or dashed lines, while the diabatic energy levels (i.e., $\Delta = 0$) are shown by the thin solid lines. The parameters $A = 10$ and $\omega = 1$ are used.

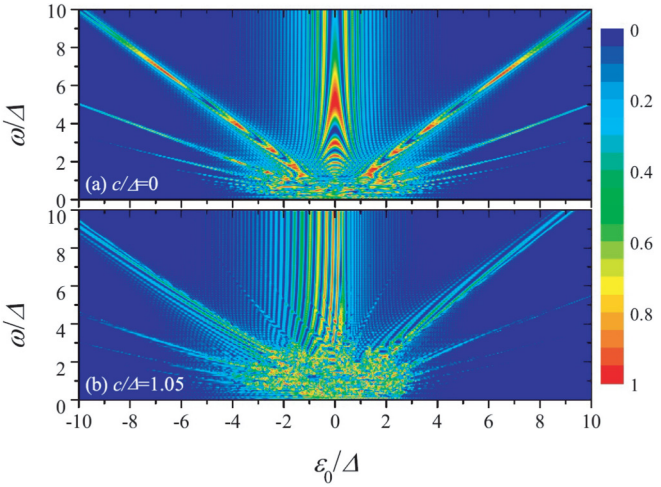

FIG. 2. Population probability $|a(t)|^2$ at time $t = 50/\Delta$ for an initial preparation of the system in the state $(a,b) = (0,1)$ at $t_0 = 0$. For numerical implementation, we have considered $A/\Delta = 2.5$ with different nonlinearities: (a) $c/\Delta = 0$ and (b) $c/\Delta = 1.05$.

where a and b are the probability amplitudes, and $\hat{\sigma}_{l=x,z}$ denote the Pauli matrices. The Hamiltonian is characterized by three parameters: the tunneling amplitude Δ, the monochromatic driving field $\gamma(t) = \epsilon_0 + A\sin\omega t$ (with amplitude A, frequency ω, and offset ϵ_0), and the nonlinear parameter c describing the dependence the level energy on the populations. The dynamics of the system is governed by the dimensionless Schrödinger equation

$$i\frac{d}{dt}\phi(t) = H(t)\phi(t), \tag{2}$$

where $\phi(t) = [a(t),b(t)]^T$ is the two-component vector. Here we have adapted the natural basis for spin operators $\hat{\sigma}_l$, namely, the diabatic basis $\{|\uparrow\rangle,|\downarrow\rangle\}$, which is formed with the eigenstates of $\hat{\sigma}_z$: $\hat{\sigma}_z|\uparrow\rangle = +|\uparrow\rangle$, $\hat{\sigma}_z|\downarrow\rangle = -|\downarrow\rangle$. It is noted that these states would be the eigenstates of the Hamiltonian if $\Delta = 0$. The adiabatic basis consists of the instantaneous eigenstates of the time-dependent Hamiltonian: $H(t)|\varphi_j(t)\rangle = E_j(t)|\varphi_j(t)\rangle$ with $j = 1,2,\ldots$, where the eigenenergies $E_j(t)$ are determined by the quartic equation

$$\sum_{l=0}^{4}\alpha_l E_j(t)^l = 0, \tag{3}$$

with the coefficients $\alpha_0 = -c^2\Delta^2/16$, $\alpha_1 = -c\Delta^2/4$, $\alpha_2 = (c^2 - \Delta^2 - \epsilon_0^2 - 2A\epsilon_0\sin\omega t - A^2\sin^2\omega t)/4$, $\alpha_3 = c$, and $\alpha_4 = 1$. The adiabatic energy levels of the system corresponding to the eigenenergies are illustrated in Fig. 1 with $\Delta = \omega = 1$ and $A = 10$. In the nonlinear case with $c/\Delta = 3$, the loop structures appear at the lower energy level for both $\epsilon_0 = 0$ and $\epsilon_0 = 5$. In the loop structure regions, the number of the eigenvalues E_j is more than two and thus the corresponding eigenstates are not orthogonal to each other. The avoided-level crossings or the loop structures occur at times $t_{1,2} + 2n\pi/\omega$ [with n being an integer, $\omega t_1 = \arcsin(-\epsilon_0/A)$, and $\omega t_2 = \pi - \omega t_1$], where the minimum gaps between the upper and lower adiabatic levels are Δ. At these times, two diabatic energy levels cross and the system undergoes sudden transitions.

III. NONLINEAR LZSM INTERFEROMETRY

For the driving system (1), we are interested in the time dependence of the population probabilities in the upper and lower energy levels. For $n = 0$ and $n = 1$, the model Hamiltonian $H(t)$ describes a full cycle of the LZSM interferometry [5] [see Fig. 1(b)], which includes three avoided-level crossings at times t_1, t_2, and $t_3 = t_1 + 2\pi/\omega$. Initially, if the nonlinear system is prepared in the state $|\downarrow\rangle$ [i.e., $(a,b) = (0,1)$] at time t_0 far from the left of t_1, then the state splits twice at times $t_{1,2}$ and recombines at time t_3, and finally, we detect the occupation probability, for instance, in the state $|\uparrow\rangle$ (i.e., $|a(t)|^2$) at time t far from the right of t_3.

The LZSM interference patterns can be destructive or constructive, which are determined by the relative phases (equal to the areas between the upper and lower energy curves) acquired during the two stages $t \in [t_1,t_2]$ and $t \in [t_2,t_3]$. In Fig. 2, we show the LZSM interference patterns formed by evolving the system from $t_0 = 0$ to $t = 50/\Delta$ with $\Delta = 1$. For the linear case [i.e., $c = 0$, see Fig. 2(a)], the interference pattern is of axial symmetry structure. However, for the nonlinear case [i.e., $c \neq 0$, see Fig. 2(b)], the axial symmetry of pattern is severely damaged. This implies that the introduction of nonlinearity in the system can strongly change the features of the LZSM interferometry. Subsequently, we will divide our discussion into four cases by comparing the characteristic frequency ω of the driving field with A and Δ to explore the effects of the nonlinearity on the interference properties.

A. Weak-coupling limit: $\Delta \ll \omega$

In the weak-coupling limit, the tunneling amplitude Δ is far less than the driving frequency ω. Thus the adiabatic energy levels at the cross points of the diabatic levels are nearly degenerate. Under this condition, the tunneling between two diabatic states $|\uparrow\rangle$ and $|\downarrow\rangle$ is weak enough to be neglected, i.e., $|a(t)|^2 \simeq |a(t_0)|^2$ and $|b(t)|^2 \simeq |b(t_0)|^2$. Based on this approximation, we can transform the system from the Schrödinger

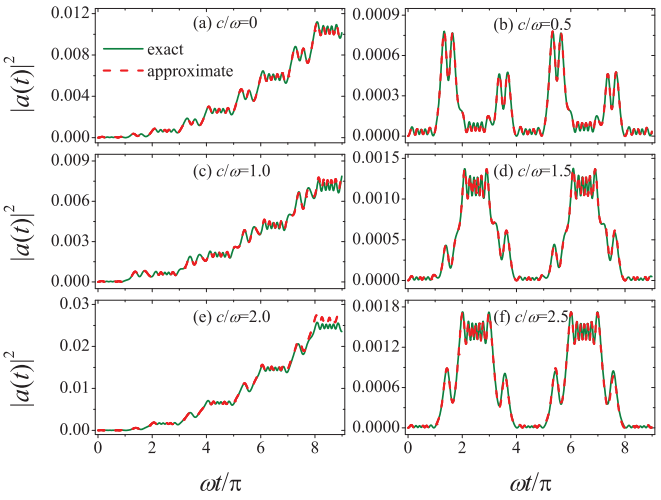

FIG. 3. Time evolution of the population probability $|a(t)|^2$ for weak coupling with different nonlinearities: (a) $c/\omega = 0$, (b) $c/\omega = 0.5$, (c) $c/\omega = 1.0$, (d) $c/\omega = 1.5$, (e) $c/\omega = 2.0$, and (f) $c/\omega = 2.5$. Olive solid lines indicate exact numerical results, while red dashed lines are approximate analytical results. For implementation, we have used $A/\omega = 10.5$, $\Delta/\omega = 0.05$, and $\epsilon_0/\omega = 3$.

picture to the Dirac picture by introducing the gauge transformation $\phi(t) = U(t)\varphi(t)$ with $U(t) = \exp\{-i[\frac{\epsilon_0}{2}t - \frac{A\cos\omega t}{2\omega} + \frac{c}{2}(|b(t_0)|^2 - |a(t_0)|^2)t]\hat{\sigma}_z\}$, with $\varphi(t) = [a'(t),b'(t)]^T$ being the new two-component vector of probability amplitudes. For the initial state $[a(t_0),b(t_0)] = [0,1]$, in the new basis the nonlinear equation (2) becomes the linear form

$$i\frac{d}{dt}\varphi(t) = \begin{pmatrix} 0 & \Omega \\ \Omega^* & 0 \end{pmatrix}\varphi(t), \tag{4}$$

with

$$\Omega = \frac{\Delta}{2}e^{i\theta(t)},\ \theta(t) = \epsilon_0 t - \frac{A}{\omega}\cos\omega t + ct, \tag{5}$$

where the symbol $*$ indicates the complex conjugate. Ω denotes the field-induced Rabi frequency which measures the effective coupling between two diabatic states with a relative phase θ. For a full cycle of LZSM interferometry, the accumulated relative phase is approximate to

$$\theta_d \simeq \int_{t_1}^{t_3}(\epsilon_0 + c - n\omega)dt = \frac{2\pi}{\omega}(\epsilon_0 + c - n\omega), \tag{6}$$

(with $n = 0,\pm1,\pm2,\ldots$) which determines the properties of the interference patterns. When $\theta_d = 2k\pi$ for any integer k, i.e., $\epsilon_0 + c \simeq (n+k)\omega = m\omega$ (with m being an integer), the interference patterns will be constructive. When $\theta_d \simeq (2k+1)\pi$, i.e., $\epsilon_0 + c \simeq (n+k+\frac{1}{2})\omega = (m+\frac{1}{2})\omega$, the interference patterns will be destructive. For example, in Fig. 3 we show the multicycle LZSM interference fringes. For $c = 0$, 1, and 2 [see Figs. 3(a), 3(c), and 3(e)], and the corresponding $\epsilon_0 + c = 3\omega$, 4ω, and 5ω, the constructive interference fringes are seen. For $c = 0.5$, 1.5, and 2.5 [see Figs. 3(b), 3(d), and 3(f)], and the corresponding $\epsilon_0 + c = (3+\frac{1}{2})\omega$, $(4+\frac{1}{2})\omega$, and $(5+\frac{1}{2})\omega$, the destructive interference fringes are seen. It should be mentioned that the exact results shown in Fig. 3 are obtained by numerical solving the nonlinear Eq. (2), while the approximate solutions are given by directly calculating the linear Eq. (4). We see that they are in good agreement for all nonlinear cases.

B. Strong-coupling limit: $\Delta \gg \omega$

In this limit the coupling between two diabatic states is much greater than the frequency of the driving field. This limit is somehow equivalent to that of adiabatic evolutions $A\omega \ll \Delta^2$. Under this condition, the tunneling between the upper and the lower adiabatic levels is small enough and can be neglected. Consider the nonadiabatic regions in the vicinity of the points $t_{1,2}$, i.e., $t = t_{1,2} + \tau$ with $\omega|\tau| \ll 1$, then the driving field γ can be linearized as follows:

$$\gamma(t_{1,2} + \tau) \simeq \pm\alpha\tau, \tag{7}$$

where the sweep rate of the control field $\alpha = A\omega|\cos\omega t_{1,2}| = A\omega\sqrt{1-(\epsilon_0/A)^2}$. Applying this approximation and keeping the notation t for the time instead of τ, the model Hamiltonian (1) can be rewritten as

$$H(t) = \frac{\Delta}{2}\hat{\sigma}_x + \frac{\alpha t + c(|b|^2 - |a|^2)}{2}\hat{\sigma}_z. \tag{8}$$

In order to show the efficiency of the above approximate treatment for adiabatic evolutions, we solve the dynamical equation (2) based on both Hamiltonian (1) and Hamiltonian (8) for the initial state $(a,b) = (0,1)$ from $t_0 = t_1 - 0.02/\alpha$ to $t = t_1 + 0.02/\alpha$. The results demonstrate that the exact solutions [obtained from Hamiltonian (1)] are coincident with the approximate ones for all nonlinear cases [given by Hamiltonian (8)] when the offset of the driving field is absent, i.e., $\epsilon_0 = 0$. However, when the offset is nonzero, the consistency of the two solutions is greatly reduced at the critical point $c/\Delta = 2$. Indeed, this critical point is determined by the condition that the balance between the interaction energy and the tunneling energy splitting is achieved [41].

When $c/\Delta < 2$, the interaction energy is less than the tunneling energy splitting and the harmonic Josephson oscillations between two diabatic states in the vicinity of the avoided level crossings occur. When $c/\Delta > 2$, the interaction energy is larger than the tunneling energy splitting and the macroscopic self-trapping phenomenon occurs, which implies the time-dependent state of (1) is one-diabatic-state dominated and thus the tunneling between two diabatic states is largely suppressed [42]. In the adiabatic limit where $\Delta^2 \gg \alpha$, for weak nonlinearity (i.e., $c/\Delta \ll 2$) the fast and large population transportation from one diabatic state to another at avoided-level-crossing points leads to very weak transitions between the adiabatic states. However, for strong nonlinearity (i.e., $c/\Delta > 2$) the small population transportation between diabatic states at avoided-level-crossing points results in apparent transitions between adiabatic states and consequently, the mixture of populations at avoided-level-crossing points makes the nonadiabatic paths interfere.

C. Weak driving limit: $A \ll \omega$

In the weak driving limit, we can employ the Jacobi-Anger relation [43]: $\exp[\pm ix\cos\omega t] = \sum_{n=-\infty}^{\infty} J_n(x)(\pm i)^n \exp[\pm in\omega t]$, where $J_n(x)$ is the nth-order

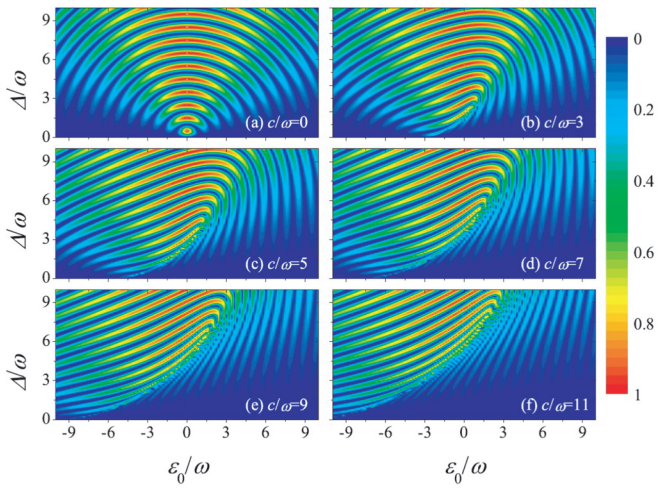

FIG. 4. LZSM interference patterns for weak driving with different nonlinearities: (a) $c/\omega = 0$, (b) $c/\omega = 3$, (c) $c/\omega = 5$, (d) $c/\omega = 7$, (e) $c/\omega = 9$, and (f) $c/\omega = 11$. Population probability $|a(t)|^2$ viewed as a function of Δ/ω and ϵ_0/ω for $A/\omega = 0.05$ from the initial time $t_0 = 0$ to $t = 2\pi/\omega$.

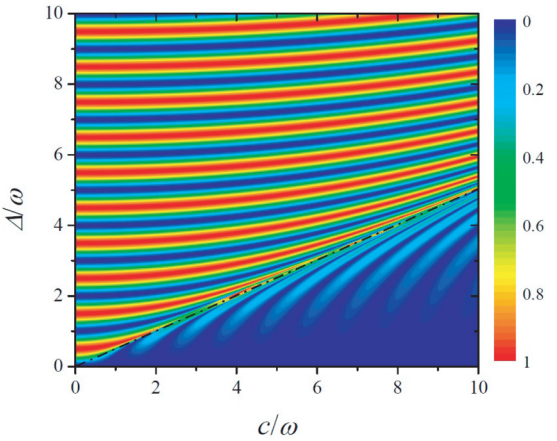

FIG. 5. Nonlinear LZSM interference patterns for weak driving at $\epsilon_0 = 0$. Population probability $|a(t)|^2$ viewed as a function of Δ/ω and c/ω for $A/\omega = 0.05$ from the initial time $t_0 = 0$ to $t = 2\pi/\omega$. Black dashed-dotted line (with slope 1/2) is plotted to denote the boundary between strong and weak oscillations.

Bessel function of the first kind with the argument x. By substituting this relation back into Eq. (5) and adopting the high-frequency approximation, Eq. (2) will be greatly simplified. In fact, the contribution of the higher-order Bessel functions is small enough and can be safely neglected [44–46]. Thus we can only keep the dominating term (i.e., the zeroth-order Bessel function), and the field-induced Rabi frequency is reduced to

$$\Omega = \frac{\Delta}{2} J_0\left(\frac{A}{\omega}\right) e^{i(\epsilon_0 + c)t}. \tag{9}$$

It must be mentioned that Eq. (9) is only valid under the condition $\Delta \ll \omega$ since we have used the approximation $|b(t)|^2 - |a(t)|^2 \simeq |b(t_0)|^2 - |a(t_0)|^2 = 1$. When $\Delta/\omega \to 0$, we find that the peaks of the resonances are located at the positions $\epsilon_0 = -c$ (see Fig. 4). Interestingly, in the linear case [see Fig. 4(a)] for $\epsilon_0 = 0$ we see that the destructive interference fringes are formed at $\Delta = k\omega$. This relation describes the multiphoton resonances, where the energy-level separation Δ is a multiple of a photon energy ω. At the nonresonant points, $\Delta = (k + \frac{1}{2})\omega$ and the constructive interference fringes are formed. For $\epsilon_0 \neq 0$, the interference pattern illustrates an axial symmetry structure.

In the nonlinear cases [see Figs. 4(b)–4(f)], the asymmetry of the interference patterns along the axis $\epsilon_0 = 0$ is seen and the asymmetry can be enlarged as the nonlinearity increases. For large Δ or c the tunneling between two diabatic states is enhanced so that the approximation $|b(t)|^2 - |a(t)|^2 \simeq |b(t_0)|^2 - |a(t_0)|^2 = 1$ cannot be applied. As a result, the nonlinear terms $c(|b(t)|^2 - |a(t)|^2)$ can strongly modify the interference properties. To describe the asymmetric behavior quantitatively, we calculate the nonlinear LZSM interference patterns for $\epsilon_0 = 0$ with different nonlinearities and illustrate the results in Fig. 5. Clearly, the oscillations can be divided into two types: strong oscillations (i.e., $|a(t)|^2 \in [0,1]$) and weak oscillations (i.e., $|a(t)|^2 \in [0,0.2]$). The boundary between these two kinds of oscillations is given by $c/\Delta = 2$, which corresponds to the critical point of self-trapping phase transition discussed previously.

D. Strong-driving limit: $A \gg \omega$

In this limit, the amplitude of the driving field A greatly exceeds the driving frequency ω and the level splitting between two adiabatic states such that the condition $A\omega \gg \Delta^2$ is always met. In this fast-driving case, we can write the field-induced Rabi frequency as follows:

$$\Omega = \frac{\Delta}{2} \sum_{-\infty}^{\infty} J_n\left(\frac{A}{\omega}\right) (-i)^n e^{i(\epsilon_0 + c - n\omega)t}. \tag{10}$$

It is easy to find that the resonance condition in the limit $\Delta/\omega \to 0$ is given by $\epsilon_0 = n\omega - c$. To show the fast-driving LZSM interferometry, we calculate the time-averaged upper diabatic state occupation probability, i.e., $\frac{1}{t-t_0}\int_{t_0}^{t} |a(t')|^2 dt'$ with $t_0 = 0$ and $t = 50\pi/\omega$. The numerical results for $A/\omega = 50$ with different nonlinear interactions are illustrated in Fig. 6. When $\Delta/\omega \to 0$ several multiphoton resonances at $\epsilon_0 = n\omega - c$ (with $n = -4, -3, \ldots, 4, 5$) are shown. When the coupling between two diabatic states increases, we find that the multiphoton-resonance peaks are broadened.

We emphasize that the introduction of the nonlinear interactions not only changes the resonance positions for weak coupling but also changes the shape of the resonant peaks. To see the details of these two effects, we evolve the system from $t_0 = 0$ to $t = 8.5\pi/\omega$ with the same initial state used previously. For $A/\omega = 10.5$ and $\Delta/\omega = 0.05$, we show the interference patterns in Fig. 7(a), which give the dependence of the final upper diabatic state occupation probability $|a(t)|^2$ on c/ω and ϵ_0/ω. Moreover, we illustrate the profiles for $\epsilon_0/\omega = 0$ and $\epsilon_0/\omega = 6$ in Figs. 7(b) and 7(c), respectively. In Fig. 7(a) it is seen that the amplitudes of the resonance peaks are different and the numbers for multiphoton resonance have an upper limit (e.g., the maximum n for $\epsilon_0 = 0$ is 13). These two features are very different from those observed in the time-averaged interference patterns. For $\epsilon_0/\omega = 6$ [see Fig. 7(c)]

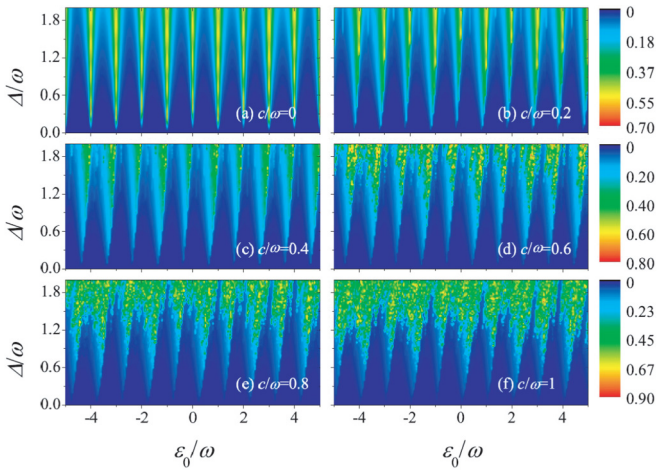

FIG. 6. LZSM interference patterns for strong driving with different nonlinearities: (a) $c/\omega = 0$, (b) $c/\omega = 0.2$, (c) $c/\omega = 0.4$, (d) $c/\omega = 0.6$, (e) $c/\omega = 0.8$, and (f) $c/\omega = 1$. Time-averaged occupation probability $\frac{1}{t-t_0}\int_{t_0}^{t} |a(t')|^2 dt'$ (with $t_0 = 0$ and $t = 50\pi/\omega$) viewed as a function of Δ/ω and ϵ_0/ω for $A/\omega = 50$.

the existence of the upper limit leads to the disappearance of the resonances in the nonlinear region $c/\omega > 7$. The resonant peaks for $\epsilon_0/\omega = 6$ [see Fig. 7(c)] are those for $\epsilon_0/\omega = 0$ [see Fig. 7(b)] moved to the left with 6ω along the c axis. In particular, a distinct deviation between the exact results based on Eq. (2) and the approximate solutions given by Eq. (4) in the strong nonlinear region [see Fig. 7(b)] is shown, which is caused by applying the approximation of $c(|b(t)|^2 - |a(t)|^2) \simeq c(|b(t_0)|^2 - |a(t_0)|^2)$.

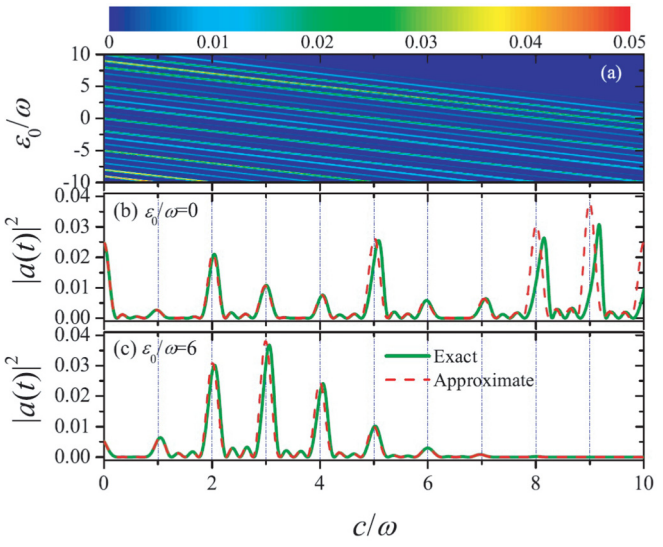

FIG. 7. (a) Nonlinear LZSM interference patterns. Final occupation probability $|a(t)|^2$ (with $t = 8.5\pi/\omega$) viewed as a function of c/ω and ϵ_0/ω for $A/\omega = 10.5$ and $\Delta/\omega = 0.05$. We also show the profiles of (a) with different ϵ_0: (b) $\epsilon_0/\omega = 0$ and (c) $\epsilon_0/\omega = 6$. Olive solid lines indicate exact numerical results, while red dashed lines are approximate analytical results.

IV. DISCUSSION AND CONCLUSION

Our nonlinear LZSM interferometry may be realized in double-well BEC systems. Under the mean-field approximation, these systems can be well described by the Gross-Pitaevskii (GP) equation $i\hbar\frac{\partial\Psi(\mathbf{r},t)}{\partial t} = [-\frac{\hbar^2\nabla^2}{2m} + V(\mathbf{r}) + g_0|\Psi(\mathbf{r},t)|^2]\Psi(\mathbf{r},t)$, where $g_0 = \frac{4\pi\hbar^2 a_s N}{m}$ with a_s, N, and m respectively being the s-wave scattering length, the total number, and mass of the atoms. For the double-well potential, the wave function can be expressed as a superposition of the two states that localize in each well separately [39,40], i.e., $\Psi(\mathbf{r},t) = \alpha(t)\psi_1(\mathbf{r}) + \beta(t)\psi_2(\mathbf{r})$. Indeed, the spatial wave functions can be obtained by using the symmetric and antisymmetric stationary eigenstates of the GP equation, and they satisfy the condition $\int \psi_i^* \psi_j d\mathbf{r} = \delta_{i,j}$ with $i,j = 1,2$. When consider a weakly linked BEC, the dynamics of the system is governed by the following Hamiltonian:

$$H(t) = \begin{pmatrix} \epsilon_1 + U|\alpha|^2 & \Omega \\ \Omega & \epsilon_2 + U|\beta|^2 \end{pmatrix}, \tag{11}$$

where $\epsilon_{1,2}$ denote the zero-point energies for two wells, Ω stands for the coupling strength between two wells, and $U = g_0\int|\psi_1|^4 d\mathbf{r} \simeq g_0\int|\psi_2|^4 d\mathbf{r}$ describes the interaction between atoms. It is easy to see that the Hamiltonian (11) is similar to the model (1) for a correspondence between $(\Delta\epsilon,\Omega,U)$ and (γ,Δ,c), with $\Delta\epsilon = \epsilon_1 - \epsilon_2$ being the energy bias. For example, we consider the experiment with ^{87}Rb BEC in [47]. The coupling strength is determined by the spacing between two wells or the height of the barrier. The atom-atom interaction can be flexibly adjusted by employing a Feshbach resonance technique. According to our theoretical proposal, when one modulates the tilt of the double wells periodically, the nonlinear LZSM interference fringes will be observed. By measuring the position shift of the fringes in the strong-driving limit, one can obtain the interaction strength and further obtain the s-wave scattering length due to the proportional relations between the three quantities.

Note that double-well BEC systems are not the only systems one can use to realize our nonlinear LZSM interferometry. Solid-state quantum devices or cold atoms in optical lattices are also the systems as possible candidates. For superconducting qubits [48–51], a nitrogen vacancy center in diamond [52], a single hole confined in a gated double quantum dot [53], and an atomic BEC in an optical lattice (with a two-band miniband structure) [54], the existing experiential results focused mainly on the weak-coupling and strong-driving regimes. However, in these systems, the nonlinear interaction between particles is usually weak and can be ignored. Therefore, to observe the effects of nonlinearity on LZSM, the systems of atomic BEC in a double-well potential would be a good choice.

In conclusion, we have investigated the nonlinear LZSM interferometry and shown that both the nonlinear interaction and the periodic driven field play an important role in the formation of interference fringes. For high-frequency driving, we have obtained the condition both of the constructive interference and the destructive interference. It is found that

the nonlinear interaction can change the level structure and result in asymmetric deformation of the interference patterns and a significant position shift of the interference fringes. Our present work provides the basis for accurately calibrating the parameters characterizing a nonlinear two-level system as well as its interactions with the external driven fields by applying the LZSM interferometry.

ACKNOWLEDGMENTS

This work is supported by the National Natural Science Foundation of China (Grants No. 11305120, No. 11665020, No. 11547046, No. 11547603, and No. 11575027) and the Natural Science Fundamental Research Program of Shaanxi Province of China (Grant No. 2015JQ1017).

[1] L. D. Landau, Phys. Z. Sowjetunion **2**, 46 (1932).
[2] G. Zener, Proc. R. Soc. London, Ser. A **137**, 696 (1932).
[3] E. C. G. Stückelberg, Helv. Phys. Acta **5**, 369 (1932).
[4] L. D. Landau, Phys. Z. Sowjetunion **1**, 88 (1932).
[5] S. N. Shevchenko, S. Ashhab, and F. Nori, Phys. Rep. **492**, 1 (2010).
[6] E. Majorana, Nuovo Cimento **9**, 43 (1932).
[7] F. Di Giacomo and E. Nikitin, Sov. Phys. Uspekhi **48**, 515 (2005).
[8] F. Forster, G. Petersen, S. Manus, P. Hänggi, D. Schuh, W. Wegscheider, S. Kohler, and S. Ludwig, Phys. Rev. Lett. **112**, 116803 (2014).
[9] E. Dupont-Ferrier, B. Roche, B. Voisin, X. Jehl, R. Wacquez, M. Vinet, M. Sanquer, and S. De Franceschi, Phys. Rev. Lett. **110**, 136802 (2013).
[10] G. Cao, H.-O. Li, T. Tu, L. Wang, C. Zhou, M. Xiao, G.-C. Guo, H.-W. Jiang, and G.-P. Guo, Nat. Commun. **4**, 1401 (2013).
[11] J. Rotvig, A. P. Jauho, and H. Smith, Phys. Rev. Lett. **74**, 1831 (1995).
[12] J. Rotvig, A. P. Jauho, and H. Smith, Phys. Rev. B **54**, 17691 (1996).
[13] L. Y. Gorelik, N. I. Lundin, V. S. Shumeiko, R. I. Shekhter, and M. Jonson, Phys. Rev. Lett. **81**, 2538 (1998).
[14] A. V. Shytov, D. A. Ivanov, and M. V. Feigel'man, Eur. Phys. J. B **36**, 263 (2003).
[15] W. Wernsdorfer, R. Sessoli, A. Caneshi, D. Gatteschi, and A. Cornia, Europhys. Lett. **50**, 552 (2000).
[16] D. A. Garanin, Phys. Rev. B **70**, 212403 (2004).
[17] C. Calero, E. M. Chudnovsky, and D. A. Garanin, Phys. Rev. B **72**, 024409 (2005).
[18] P. Földi, M. G. Benedict, J. M. Pereira, and F. M. Peeters, Phys. Rev. B **75**, 104430 (2007).
[19] P. Földi, M. G. Benedict, and F. M. Peeters, Phys. Rev. A **77**, 013406 (2008).
[20] G. D. Fuchs, V. V. Dobrovitski, D. M. Toyli, F. J. Heremans, and D. D. Awschalom, Science **326**, 1520 (2009).
[21] M. B. Kenmoe and L. C. Fai, Phys. Rev. B **94**, 125101 (2016).
[22] B. K. Cooper and V. M. Yakovenko, Phys. Rev. Lett. **96**, 037001 (2006).
[23] A. Banerjee and V. M. Yakovenko, Phys. Rev. B **78**, 125404 (2008).
[24] M. Mark, T. Kraemer, P. Waldburger, J. Herbig, C. Chin, H.-C. Nägerl, and R. Grimm, Phys. Rev. Lett. **99**, 113201 (2007).
[25] M. Mark, F. Ferlaino, S. Knoop, J. G. Danzl, T. Kraemer, C. Chin, H.-C. Nägerl, and R. Grimm, Phys. Rev. A **76**, 042514 (2007).
[26] C. S. E. van Ditzhuijzen, A. Tauschinsky, and H. B. van Linden van den Heuvell, Phys. Rev. A **80**, 063407 (2009).
[27] Q. Zhang, P. Hänggi, and J. B. Gong, Phys. Rev. A **77**, 053607 (2008).
[28] Q. Zhang, P. Hänggi, and J. B. Gong, New J. Phys. **10**, 073008 (2008).
[29] L. Du, M. Wang, and Y. Yu, Phys. Rev. B **82**, 045128 (2010).
[30] J.-N. Zhang, C.-P. Sun, S. Yi, and F. Nori, Phys. Rev. A **83**, 033614 (2011).
[31] B. T. Torosov and N. V. Vitanov, Phys. Rev. A **96**, 013845 (2017).
[32] Q. Xie, Phys. Rev. A **97**, 022113 (2018).
[33] B. Wu and Q. Niu, Phys. Rev. A **61**, 023402 (2000).
[34] J. Liu, L. Fu, B. Y. Ou, S. G. Chen, D. I. Choi, B. Wu, and Q. Niu, Phys. Rev. A **66**, 023404 (2002).
[35] D. F. Ye, L. B. Fu, and J. Liu, Phys. Rev. A **77**, 013402 (2008).
[36] L. B. Fu, D. F. Ye, C. Lee, W. Zhang, and J. Liu, Phys. Rev. A **80**, 013619 (2009).
[37] S. C. Li, L. B. Fu, W. S. Duan, and J. Liu, Phys. Rev. A **78**, 063621 (2008).
[38] S. C. Li, J. Phys. B: At. Mol. Opt. Phys. **43**, 205303 (2010).
[39] A. Smerzi, S. Fantoni, S. Giovanazzi, and S. R. Shenoy, Phys. Rev. Lett. **79**, 4950 (1997).
[40] S. Raghavan, A. Smerzi, S. Fantoni, and S. R. Shenoy, Phys. Rev. A **59**, 620 (1999).
[41] C. Ottaviani, V. Ahufinger, R. Corbalán, and J. Mompart, Phys. Rev. A **81**, 043621 (2010).
[42] F. K. Abdullaev and R. A. Kraenkel, Phys. Lett. A **272**, 395 (2000).
[43] A. Erdelyi, W. Magnus, F. Oberhettinger, and F. G. Tricomi, *Higher Transcendental Functions* (McGraw-Hill, New York, 1953).
[44] A. Eckardt, C. Weiss, and M. Holthaus, Phys. Rev. Lett. **95**, 260404 (2005).
[45] Y. Kayanuma, Phys. Rev. A **50**, 843 (1994).
[46] Y. Kayanuma and Y. Mizumoto, Phys. Rev. A **62**, 061401(R) (2000).
[47] T. Berrada, S. van Frank, R. Bücker, T. Schumm, J.-F. Schaff, J. Schmiedmayer, B. Julía-Díaz, and A. Polls, Phys. Rev. A **93**, 063620 (2016).
[48] W. D. Oliver, Ya. Yu, J. C. Lee, K. K. Berggren, L. S. Levitov, and T. P. Orlando, Science **310**, 1653 (2005).
[49] M. Sillanpää, T. Lehtinen, A. Paila, Yu. Makhlin, and P. Hakonen, Phys. Rev. Lett. **96**, 187002 (2006).
[50] C. M. Wilson, T. Duty, F. Persson, M. Sandberg, G. Johansson, and P. Delsing, Phys. Rev. Lett. **98**, 257003 (2007).
[51] A. Izmalkov, S. H. W. van der Ploeg, S. N. Shevchenko, M. Grajcar, E. Il'ichev, U. Hübner, A. N. Omelyanchouk, and H.-G. Meyer, Phys. Rev. Lett. **101**, 017003 (2008).
[52] L. Childress and J. McIntyre, Phys. Rev. A **82**, 033839 (2010).
[53] A. Bogan, S. Studenikin, M. Korkusinski, L. Gaudreau, P. Zawadzki, A. S. Sachrajda, L. Tracy, J. Reno, and T. Hargett, Phys. Rev. Lett. **120**, 207701 (2018).
[54] S. Kling, T. Salger, C. Grossert, and M. Weitz, Phys. Rev. Lett. **105**, 215301 (2010).